J Mater Sci (2013) 48:2681–2689
DOI 10.1007/s10853-012-7063-1

Interface characterization and thermal degradation of ferrite/poly(vinylidene fluoride) multiferroic nanocomposites

P. Martins · C. M. Costa · M. Benelmekki · G. Botelho · S. Lanceros-Méndez

Received: 20 October 2012 / Accepted: 30 November 2012 / Published online: 11 December 2012

Abstract Flexible multiferroic 0–3 composite films, with $CoFe_2O_4$, $Ni_{0.5}Zn_{0.5}Fe_2O_4$ or $NiFe_2O_4$ ferrite nanoparticles as filler and polyvinylidene fluoride (PVDF) as the polymer matrix, have been prepared by solvent casting and melt crystallization. The inclusion of ferrite nanoparticles in the polymer allows to obtain magnetoelectric nanocomposites through the nucleation of the piezoelectric β-phase of the polymer by the ferrite fillers. Since the interface between PVDF and the nanoparticles has an important role in the nucleation of the polymer phase, thermogravimetric analysis was used in order to identify and quantify the interface region and to correlate it with the β-phase content. It is found that an intimate relation exists between the size of the interface region and the piezoelectric β-phase formation that depends on the content and type of ferrite nanoparticles. The interface value and the β-phase content increase with increasing ferrite loading and they are higher for $CoFe_2O_4$ and $Ni_{0.5}Zn_{0.5}Fe_2O_4$ ferrite nanoparticles. The composites shows lower thermal stability than the pure polymer due to the existence of mass loss processes at lower temperature than the main degradation of the polymer. The main degradation of the polymer matrix, nevertheless, shows increased degradation temperature with increasing ferrite content.

P. Martins · C. M. Costa · M. Benelmekki · S. Lanceros-Méndez (✉)
Centro/Departamento de Física da Universidade do Minho, Campus de Gualtar, 4710-057 Braga, Portugal
e-mail: lanceros@fisica.uminho.pt

G. Botelho
Centro/Departamento de Química da Universidade do Minho, Campus de Gualtar, 4710-057 Braga, Portugal

S. Lanceros-Méndez
INL-International Iberian Nanotechnology Laboratory, 4715-330 Braga, Portugal

Introduction

Poly(vinylidene fluoride), PVDF, is a semi-crystalline polymer that can crystallize in four crystalline phases known as α, β, δ, and γ [1, 2]. The α and β phases are the most interesting ones for technological applications and, therefore, the most studied. The α-phase is non-polar, it has a *trans* and *gauche*-bond (*TGTG′*) chain conformation and it is typically obtained by cooling from the melt. The β-phase is piezo-, pyro-, and ferroelectric. It has an *all-trans* conformation (*TTTT*) resulting in a net dipole moment within the unit cell [2, 3].

Due to its electroactive properties β-PVDF finds increasing applications for sensors and actuators, batteries, and in the biomedical field [4, 5].

As the piezoelectric β-phase is the most interesting from the technological point of view and its presence in the polymer depends on the processing conditions [1, 6], different approaches have been used to obtain this phase.

Most often, the polar β-phase is obtained by uniaxial or biaxial stretching of α-phase films at temperatures between 70 and 100 °C and stretch ratios of three to five [2, 7]. It has been also obtained by crystallization from dimethyl formamide (DMF) or dimethyl acetamide (DMAc) solutions at temperatures below 70 °C [7, 8], but this method leads to porous and fragile films [7].

Other methods used to obtain piezoelectric β-phase samples with good mechanical properties are the incorporation of clays [9], zirconia [10], carbon nanotubes [11], ferrite nanoparticles [12], and silver nanoparticles [13] within the polymer matrix, among others.

Particularly interesting is the incorporation of ferrite nanoparticles as, together with the nucleation of the piezoelectric β-phase, it leads to the development of magnetoelectric (ME) composites, with interesting applications in the areas of sensor and actuator due to the interplay of the magnetostriction of the ferrites and the piezoelectricity of the polymer matrix [14, 15].

With the addition of such nanofillers the polymer thermal properties can be changed, which can in turn modify the application range of the materials [16–18]. In this way, the understanding of how thermal properties are changed due the physical and chemical interaction between nanoparticles and polymer is essential. Further, by addressing how nanoparticles induce variations in the thermal properties and thermal degradation of polymers, valuable information on the nature of the particle/polymer interactions can be obtained [19, 20]. Thermogravimetric analysis (TG) is typically used to evaluate the thermal degradation of polymers and polymer composites [21–23]. In particular, it has been proven that in PVDF the thermal degradation occurs in two steps, independent of the phase of the sample [24]. Further, the thermal stability of the material has been improved by suitable nanofillers, such as clays [25]. Similar findings were obtained in $CaCO_3$/PVDF composites [26].

Since the thermal degradation and the nucleation of the ferroelectric phase is strongly influenced both by geometrical factors due to the nanosize of the fillers and, in particular, by the interactions in the interface between nanofillers and PVDF [27], TG appears as one of the most suitable techniques to study the nanoparticle/polymer interface effects [28].

In this work, $CoFe_2O_4$, $Ni_{0.5}Zn_{0.5}Fe_2O_4$, and $NiFe_2O_4$ nanoparticles were incorporated into the PVDF matrix with different filler contents as they have proven to be able to nucleate the piezoelectric phase of the polymer. The influence of filler type and content in the nucleation of the β-phase of the polymer has been correlated to the variations in the thermal degradation of the composite.

Materials and methods

Materials

Poly(vinylidene fluoride), PVDF, (Solef 1010) powder was supplied by Solvay. Ferrite nanoparticles and *N,N* dimethylformamide (DMF) were purchased from Nano-Amor and Sigma-Aldrich, respectively, and used as received. $CoFe_2O_4$, $NiFe_2O_4$, and $Ni_{0.5}Zn_{0.5}Fe_2O_4$ ferrite nanoparticles have dimensions between 35–55 nm, 20–30 nm, and 10–30 nm, respectively [29].

Methods

In order to obtain a good filler dispersion, a solution of ferrite nanoparticles in DMF was first placed in an ultrasound bath for 6 h. After this period of time, PVDF powder was added to the solution. Complete dissolution of the polymer was achieved with the help of a Teflon mechanical stirrer incorporated in the ultrasound bath during 1 h.

Flexible composite films with an average thickness of ~50 μm and ferrite weight percentages (wt%) from 0.01 to 50 (from 3×10^{-5} to 0.25 in volume fraction) were obtained by spreading the solution at room temperature on a clean glass substrate. Solvent evaporation was obtained inside an oven at a controlled temperature of 210 °C [7].

The vibrational modes of the polymer used to determine the polymer phase and phase content were recorded by Fourier transformed infrared spectroscopy (FTIR) using a Perkin-Elmer Spectrum 100 in ATR from 650 to 4000 cm^{-1} with a resolution of 4 cm^{-1}. 32 scans were performed for each sample.

The thermal behavior of the samples was determined by TG. Samples were transferred to open ceramic crucibles with capacity of 60 μL and analyzed using a Pyris 1 TG Perkin-Elmer thermobalance operating between 50 and 850 °C. A heating rate of 10 ± 0.2 °C min^{-1} and a nitrogen flow rate of 50 mL min^{-1} were used.

The existence of a nanoparticle/polymer interphase located at the interface was investigated by transmission electron microscopy (TEM) imaging using a JEOL JEM-1210 electron microscope operating at 200 keV. The samples were embedded in an epoxy resin and cut into thin films of about 100 nm using a Leica Ultracut UCT Ultramicrotome.

Theoretical background

PVDF has characteristic infrared bands such as the ones at 766 and 840 cm^{-1} that have been identified to correspond to the α- and β-phase, respectively [3, 30]. The variation of those bands as a function of ferrite nanoparticle wt% was analyzed and the phase content was quantified applying Eq. 1 [6, 31]:

$$F(\beta) = \frac{X_\beta}{X_\alpha + X_\beta} = \frac{A_\beta}{(K_\beta/K_\alpha)A_\alpha + A_\beta}, \quad (1)$$

where $F(\beta)$ represents the β-phase content; A_α and A_β are the absorbencies at 766 and 840 cm^{-1}, corresponding to the α and β-phase material; K_α and K_β are the absorption coefficient at the respective wavenumber; and X_α and X_β are the degree of crystallinity of each phase. The value of K_α is 6.1×10^4 and the value of K_β is 7.7×10^4 cm^2 mol^{-1} [32, 33].

The influence the ferrite nanoparticles in the polymer thermal degradation was determined by two different methods [34, 35]. First, the Broido method was used, assuming $n = 1$ and considering the specific heating rate $\beta = \partial T/\partial t$ [36]:

$$\ln[-\ln(1-\alpha)] = -\frac{E_a}{RT} + \text{const}, \quad (2)$$

where α represents the degree of conversion of the sample under degradation, defined by $\alpha = w_0 - w(t)/w_0 - w_\infty$. Here, w_0, w_t and w_∞ are the weights of the sample before degradation, at time t and after complete degradation, respectively. E_a is the activation energy of the process, T is the temperature, and R is the gas constant (8.314 J mol^{-1} K^{-1}).

Further, the Coats–Redfern method [37] was also used, considering a constant heating rate:

$$\ln\left[\frac{-\ln(1-\alpha)}{T^2}\right] = -\frac{E_a}{RT} + \ln\frac{AR}{\beta E_a}, \quad (3)$$

where A is constant, β is the heating rate and α represents the degree of conversion.

The dependence of the maximum weight loss degradation temperature of the polymer on the ferrite nanoparticle concentration is described by Eq. 4 [28]:

$$T_I = T_1 + T_2 \exp(Cx), \quad (4)$$

where T_1, T_2 and C are fitting constants and x is the weight fraction of ferrite nanoparticles. Here, $T_1 + T_2 = T_I^0$, where T_I^0 is the temperature at which the weight loss of the pristine polymer is maximum.

In polymer nanocomposites, the interface between the polymer and nanoparticles has an important role in determining the final properties of the material. Through TG it is possible to evaluate the mass fraction of the polymer located at the interface, m_I, using the following equation [28]:

$$m_I = \frac{m(x)_{I0} - m_{I0}}{m_{I0}} \times 100, \quad (5)$$

where m_{I0} is the mass of the pristine polymer at the temperature at which the mass loss rate is maximum and $m(x)_{I0}$ is the mass of the composite containing a given wt% of nanoparticles that has not degraded at the temperature at which the mass loss rate of the pristine polymer is maximum.

Results and discussion

FTIR spectra (not shown) have been previously used to quantify the crystalline phase type and content in the polymer as described in detail in [12]. Figure 1 presents the variation of β-phase content with increasing ferrite concentration.

Figure 1 reveals that the β-phase content depends not only on the ferrite content but also on the type of ferrite nanoparticle. $CoFe_2O_4$ and $Ni_{0.5}Zn_{0.5}Fe_2O_4$ nanoparticles induce an almost complete β-phase formation for ferrite weight contents lower than 5 %. However, in the case of $NiFe_2O_4$ nanoparticles, the β-phase nucleation just starts for ferrite contents higher than 5 wt%.

The β-phase nucleation depends on the nanoparticle-polymer electrostatic interactions and it is also related to the formation of an interphase region as explained in [29].

TG thermograms and the corresponding differential TG plots (DTG) for different $CoFe_2O_4$ nanoparticle concentrations, ranging from 0 to 50 wt%, are shown in Fig. 2.

In all cases, the typical two step thermal degradation characteristic of PVDF [24] is verified. The first step of degradation of the polymer occurs between 400 and 500 °C, the polymer maximum degradation temperature being influenced by the nanoparticle content present in the nanocomposite. In this first degradation step the decomposition mechanism is chain-stripping where carbon-hydrogen and carbon fluorine scission occurs and the presence of both hydrogen and fluorine radicals leads to the formation of hydrogen fluoride [24, 38]. The formation of

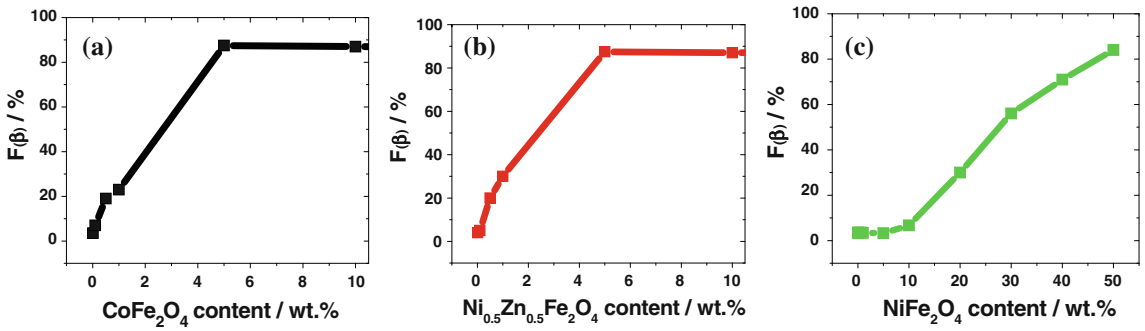

Fig. 1 Evolution of the β-phase content with increasing filler concentration for, **a** $CoFe_2O_4$/PVDF, **b** $Ni_{0.5}Zn_{0.5}Fe_2O_4$/PVDF, and **c** $NiFe_2O_4$/PVDF nanocomposites

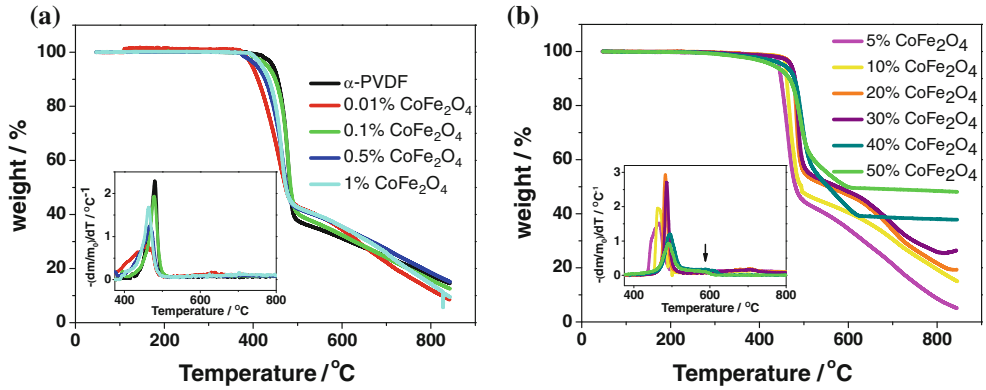

Fig. 2 TG thermograms of $CoFe_2O_4$/PVDF nanocomposites for **a** small ferrite contents and **b** large ferrite contents. An *arrow* identifies an additional degradation step with respect to the pristine polymer in the DTG representation

this compound is responsible for the weight loss observed in the first degradation step.

The second degradation step occurs between 500 and 850 °C, and the differences observed in the plots comparative to the pure α-phase PVDF are to be ascribed to the presence of ferrite nanoparticles, as the different phases of PVDF show similar thermal degradation characteristics [39]. This second step is a complex degradation process resulting in poly(aromatization). The polyenic sequence formed previously on the first degradation step is unstable and, as a consequence, the macromolecules formed undergo further reactions leading to scission followed by the formation of aromatic molecules [24, 40].

The residual weight that remains at 850 °C corresponds mainly to the ferrite nanoparticles together with the residual char from the previous degradation steps.

An additional degradation step (identified as 3rd step in Table 1) with respect to the pure polymer is also identified in the multiferroic nanocomposite samples. This step is particularly well identified in the derivative of the TG curves (DTG) (Fig. 2, inset). The emergence of a new stage of degradation in comparison to the pure polymer is related to the increase of an interphase in the interface volume between nanoparticles and polymer, related to the nucleation of the polymer β-phase [29].

The onset temperature for neat PVDF (458 °C) is lower than those of $CoFe_2O_4$/PVDF nanocomposites with ferrite contents higher than 1 wt% (≈475 °C), indicating that the thermal stability of the matrix has been improved with the addition of $CoFe_2O_4$ nanoparticles [41].

TG plots presented in the Fig. 3a, b show the thermal stability of the polymer with increasing $NiFe_2O_4$ and $Ni_{0.5}Zn_{0.5}Fe_2O_4$ ferrite nanoparticle content, respectively.

Similar to the $CoFe_2O_4$/PVDF composites, the typical two steps thermal degradation characteristic of the polymer is observed for the samples with low ferrite nanoparticle content. With increasing ferrite content an additional degradation step emerges at temperatures around 600 °C, which is related to the interaction between the nanoparticles and the polymer matrix [29]. In this case, for temperature above 800 °C and high filler loading contents, residuals are about 4 % lower than the original ferrite nanoparticle loading, indicating some mass loss with respect to the original nanofiller content which is to be ascribed to impurities related to the nanoparticle preparation.

In the same way as observed for the $CoFe_2O_4$/PVDF composites, the onset temperature for neat PVDF (458 °C) is again lower than those for $NiFe_2O_4$/PVDF and $Ni_{0.5}Zn_{0.5}Fe_2O_4$/PVDF nanocomposites with ferrite contents higher than 1 wt% (≈480 °C), indicating that the thermal stability of the matrix has been improved with the addition of the nanoparticles [41].

This behavior can be explained by the presence of the char formed from the PVDF matrix, which is further stabilized through π–π electronic interactions with the ferrite nanoparticles [10, 42]. Due to the fine dispersion and good thermal properties, the ferrite nanoparticles might strongly hinder the volatility of the decomposed products and limit the continuous decomposition of the PVDF [43].

A small loss mass at around 200 °C (Figs. 2, 3) in the nanocomposites that does not exist in the pure polymer matrix is also noted. This mass loss is commonly found in polymer/nanoparticle composites hybrid films [44] and it is ascribed to the evaporation of residual solvent and/or physically absorbed water [45]. In the present case, the amount of mass loss seems to be too large to be just attributed to the aforementioned situations and, therefore, some catalytic degradation seems to be induced at ∼200 °C by the presence of the nanoparticles. This degradation can be induced by the different thermal characteristics of ferrite fillers and polymer will lead to larger local temperatures in the polymer/nanoparticle interface than in the rest of the polymer and, therefore, to earlier degradation of the polymer at that region when compared to the average sample temperature. The increase in the onset temperature and a small decrease in thermal stability

Table 1 Parameters determined by TG analysis for the different nanocomposites

Sample	Degradation stage	Td (°C)	Interface (%)	Weight loss (%)	Activation energy	
					Broido (kJ mol^{-1})	Coats–Redfern (kJ mol^{-1})
a-PVDF	1st step	480	0	62	303	283
	2nd step	–	–	23	23	22
0.01 % $CoFe_2O_4$	1st step	450	18	55	138	109
	2nd step	–	–	36	17	15
0.1 % $CoFe_2O_4$	1st step	477	11	59	192	203
	2nd step	–	–	25	17	17
0.5 % $CoFe_2O_4$	1st step	467	5	55	163	143
	2nd step	–	–	30	17	11
1 % $CoFe_2O_4$	1st step	463	14	56	212	191
	2nd step	–	–	34	19	10
5 % $CoFe_2O_4$	1st step	463	25	52	386	321
	2nd step	714	–	22	17	10
	3rd step	–	–	41	20	10
10 % $CoFe_2O_4$	1st step	470	28	51	445	468
	2nd step	712	–	16	13	10
	3rd step	–	–	8	25	22
20 % $CoFe_2O_4$	1st step	483	33	43	468	418
	2nd step	649	–	26	14	20
	3rd step	–	–	10	52	35
30 % $CoFe_2O_4$	1st step	486	37	42	483	416
	2nd step	649	–	22	16	8
	3rd step	–	–	5	59	38
40 % $CoFe_2O_4$	1st step	494	35	38	290	256
	2nd step	590	–	20	58	46
	3rd step	–	–	2	19	12
50 % $CoFe_2O_4$	1st step	491	33	34	223	214
	2nd step	594	–	13	60	40
	3rd step	–	–	1	14	25
5 % $NiFe_2O_4$	1st step	484	16	60	378	277
	2nd step	–	–	23	21	19
10 % $NiFe_2O_4$	1st step	476	16	49	446	401
	2nd step	–	–	21	16	13
20 % $NiFe_2O_4$	1st step	494	18	44	372	317
	2nd step	–	–	28	23	17
30 % $NiFe_2O_4$	1st step	506	19	41	262	241
	2nd step	625	–	18	36	18
	3rd step	–	–	13	27	21
40 % $NiFe_2O_4$	1st step	507	19	29	168	182
	2nd step	591	–	16	58	30
	3rd step	–	–	10	36	17
50 % $NiFe_2O_4$	1st step	509	30	21	151	102
	2nd step	598	–	19	82	60
	3rd step	–	–	6	31	16
5 % $Ni_{0.5}Zn_{0.5}Fe_2O_4$	1st step	478	26	54	295	294
	2nd step	625	–	7	17	12
	3rd step	–	–	3	21	27

Table 1 continued

Sample	Degradation stage	Td (°C)	Interface (%)	Weight loss (%)	Activation energy	
					Broido (kJ mol^{-1})	Coats–Redfern (kJ mol^{-1})
10 % $Ni_{0.5}Zn_{0.5}Fe_2O_4$	1st step	489	28	54	392	400
	2nd step	627	–	10	13	10
	3rd step	–	–	4	19	24
20 % $Ni_{0.5}Zn_{0.5}Fe_2O_4$	1st step	502	28	50	326	341
	2nd step	575	–	6	11	8
	3rd step	–	–	5	15	13
30 % $Ni_{0.5}Zn_{0.5}Fe_2O_4$	1st step	505	35	40	193	198
	2nd step	568	–	6	16	12
	3rd step	–	–	5	17	16
40 % $Ni_{0.5}Zn_{0.5}Fe_2O_4$	1st step	506	38	33	143	149
	2nd step	533	–	8	69	52
	3rd step	–	–	10	19	20
50 % $Ni_{0.5}Zn_{0.5}Fe_2O_4$	1st step	507	38	23	126	92
	2nd step	561	–	16	145	97
	3rd step	–	–	9	18	30

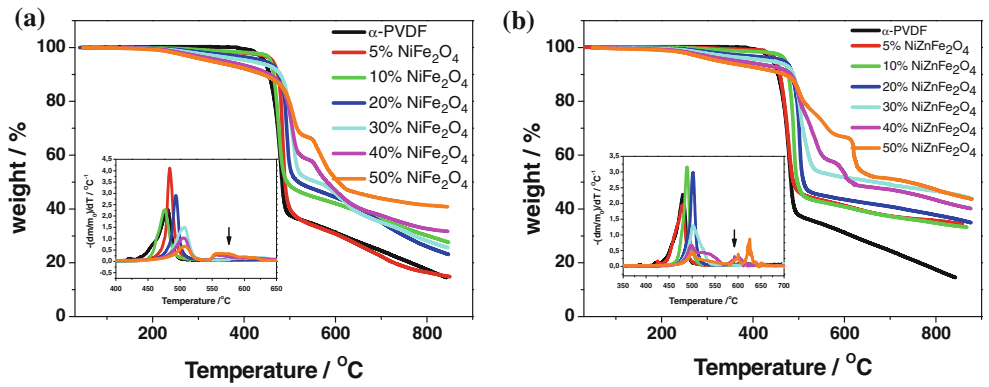

Fig. 3 TG thermograms a function of the ferrite content for **a** $NiFe_2O_4$/PVDF and **b** $Ni_{0.5}Zn_{0.5}Fe_2O_4$/PVDF. The *inset* shows the corresponding DTG curves. An *arrow* identifies an additional degradation step

around 200 °C found in the ferrite/PVDF nanocomposites has also been reported by Pal et al. [10] in Zirconia-coated carbon nanotube/PVDF nanocomposites. Due to this lower temperature mass loss, it can be stated that the composites show an overall lower thermal stability with respect to mass loss than the pure polymer, even when the main thermal degradation of the polymer matrix is increased.

The thermal degradation was studied by the Broido method, in which a straight line is observed in the plot of $\ln[-\ln(1-\alpha)]$ versus T^{-1} with a slope of $-E_a R^{-1}$, from which the activation energy is determined [46] (Fig. 4a).

In an analogous way, analysis of the TG curves was performed with the Coats–Redfern method by plotting $\ln[-\ln(1-\alpha)/T^2]$ versus T^{-1} and determining the activation energy of the nanocomposites [47] (Fig. 4b).

Table 1 shows a compilation of the data obtained from the TG measurements for the different composites, e.g., the degradation temperature, the interface value determined through Eqs. 4 and 5, and the kinetic parameters obtained from Broido (Eq. 2) and Coats–Redfern (Eq. 3) methods.

In low lower ferrite content $CoFe_2O_4$/PVDF composites (0.01–1 wt%), nanoparticles act as polymer matrix defects decreasing the value of the activation energy. For all nanocomposites with ferrite contents above 5 %, the activation energy increases with increasing ferrite content until reaching a maximum and then decreases. It is known that the addition of nanofillers can lead to thermal stabilization of polymers during their decomposition [48]. In the present investigation, a thermal stability enhancement has been observed at intermediate nanoparticle loadings while at

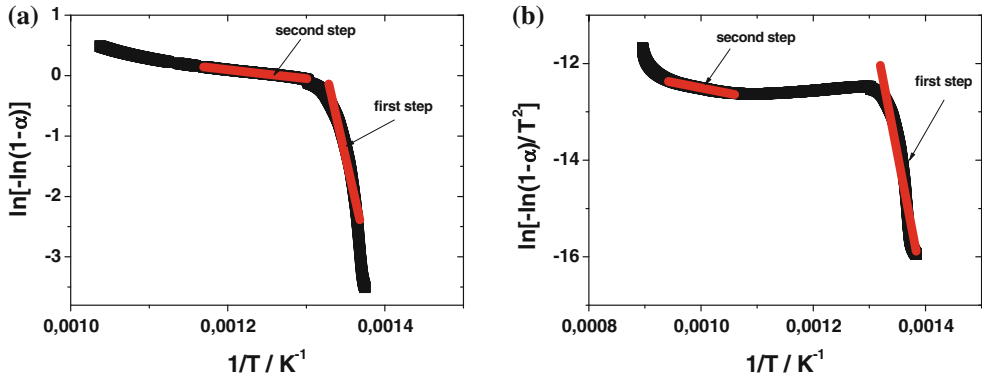

Fig. 4 Representation of the data of Fig. 2 for the sample with 1 wt% of $CoFe_2O_4$ in order to apply the **a** Broido method and the **b** Coats–Redfern method

higher contents thermal stability becomes progressively lower [49]. At the lower concentrations, the α to β polymer phase transformation induced by the electrostatic interactions between the C–F bands of PVDF and the ferrite nanoparticles improves the thermal stability of PVDF [50]. On the other hand, the formation of aggregates at high nanoparticle concentrations and the existence of high ferrite content will fade the beneficial effects of nucleation of the β-phase with respect to thermal stability as the presence of such large amounts of fillers leads to variations in the connectivity of the polymer phase as well as strong effects in the internal heat transfer kinetics due to the different thermal characteristics of the nanoparticles and the polymer.

The observed difference in the activation energy values obtained from the Broido and Coats–Redfern methods is attributed to the different mathematical approaches used to calculate the kinetic parameters [35, 51]. The correlation coefficients are 0.984 and 0.975, respectively, and the observed trend obtained by the two methods is the same.

Further, variations in the DTG temperature as a function of ferrite nanoparticle content are represented in Fig. 5. The fitting for each ferrite/PVDF nanocomposite with Eq. 4 is also shown.

For all nanocomposites, the addition of ferrite nanoparticles leads to the enhancement of the thermal stability of the main degradation of the polymer which is demonstrated by the increase of the polymer DTG temperature with increasing ferrite nanoparticle loading.

It is well known that the polymer thermal degradation begins with the generation of free radicals, which are transferred to the adjacent chains by intermolecular and intramolecular chain reaction, followed by a termination step [52]. Ferrite nanoparticles may act as radical scavengers that largely suppress these chain transfer reactions and prevent polymer chains from decomposing, that is to say, the rate of bubble nucleation decreases and it needs more time for the volatiles to reach a critical concentration. Therefore, DTG temperature of a nanocomposite is higher in comparison to neat PVDF [53].

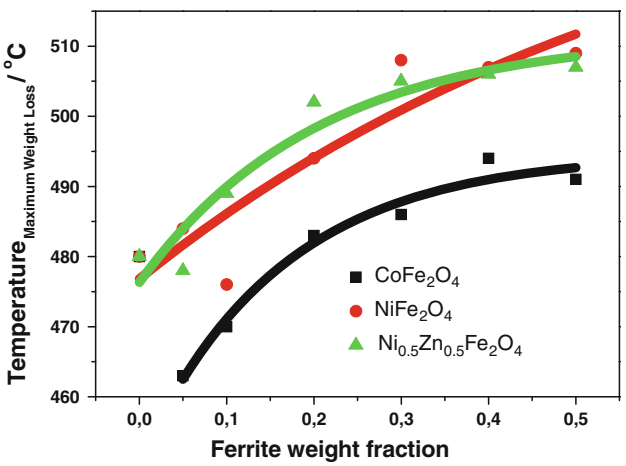

Fig. 5 Maximum degradation temperature versus ferrite nanoparticle content and the respective fitting curves with Eq. 4

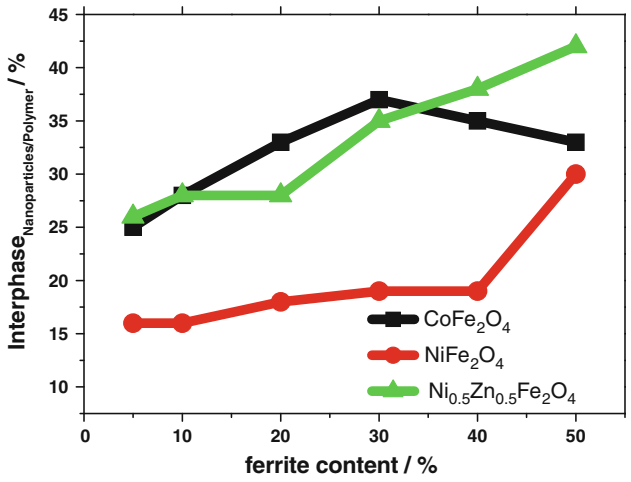

Fig. 6 Evolution of the interface volume between nanoparticles and polymer as a function of ferrite nanoparticles content

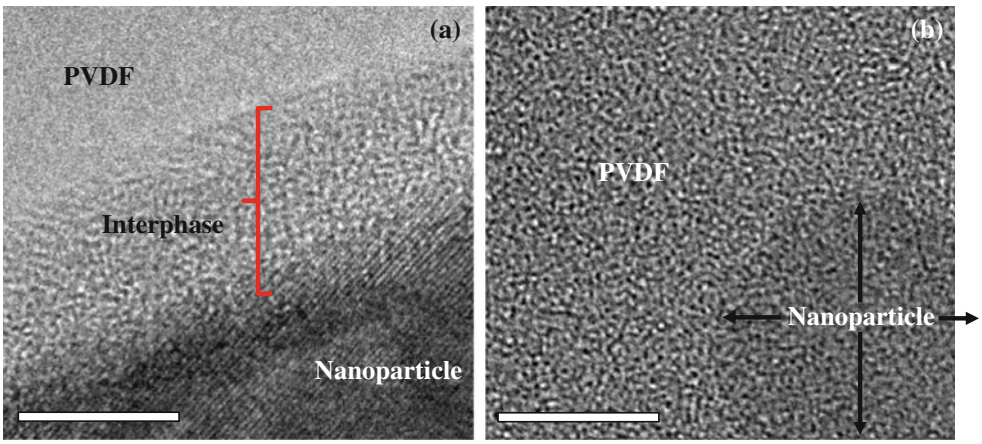

Fig. 7 TEM images of ferrite/PVDF (95/5 wt%) nanocomposites with: **a** $CoFe_2O_4$ nanoparticles and **b** $NiFe_2O_4$ nanoparticles. The *scale bar* corresponds to 10 nm

In Fig. 6, the variations in the volume fraction of the polymer at the interface region, obtained with Eq. 5, as a function of ferrite concentration are represented.

An increase of the interface value with increasing ferrite loading is observed for all composites. The size of the interphase between ferrite nanoparticles and polymer is significantly affected by the quantity and type of ferrite nanoparticle.

The interface value increases with increasing ferrite loading and it is larger for $CoFe_2O_4$ and $Ni_{0.5}Zn_{0.5}Fe_2O_4$ ferrite nanoparticles in comparison to $NiFe_2O_4$ ones, indicating that the quantity of the interface also depends on the ferrite type.

With increasing interface value, the interaction between the partially positive CH_2 bonds of the PVDF chains and the electrostatically negative charged ferrites will be promoted, explaining the fact that the electroactive β-phase nucleation is higher for the nanocomposites that have higher interface values [29].

The existence of a nanoparticle/polymer interphase is distinctly confirmed by TEM in the $CoFe_2O_4$/PVDF (95/5 wt%) nanocomposites (Fig. 7).

Figure 7 reveals a significant dissimilarity between the two nanocomposites: while a well distinguished interphase between the ferrite nanoparticle and the polymer is observed for the $CoFe_2O_4$/PVDF nanocomposites (a), the existence of such interphase is not observed in the $NiFe_2O_4$/PVDF nanocomposites (b). This observation is in agreement with the results presented in Figs. 1 and 6, since the nucleation of the electroactive β-phase in $NiFe_2O_4$/PVDF nanocomposites starts from the 5 wt% and the interface value is higher for $CoFe_2O_4$ in comparison to $NiFe_2O_4$ ones. It is noticed here that the interface volume, as defined by Eq. 5 is not necessarily equal to the interphase region observed by TEM, as they are based on different physical principles. It is relevant to notice that a larger calculated interface region (Fig. 6), e.g., larger interaction volume, is correlated to larger observed interphase volume (Fig. 7).

Conclusions

Composite films of different ferrites nanoparticles, $CoFe_2O_4$, $Ni_{0.5}Zn_{0.5}Fe_2O_4$, and $NiFe_2O_4$, and PVDF fluoride have been prepared in order to obtain multiferroic composites through the nucleation of the piezoelectric β-phase of the polymer by the ferrite fillers. TG was used to study the thermal stability of the composites and to quantify the interface region leading to the β-phase nucleation.

It was found that the size of the interface between the ferrite nanoparticles and the polymer is significantly affected by the content and type of ferrite nanoparticles. The interface value and the β-phase content increases with increasing ferrite loading and it is higher for the $CoFe_2O_4$ and $Ni_{0.5}Zn_{0.5}Fe_2O_4$ fillers in comparison to the $NiFe_2O_4$ ones, indicating that the value of the size of the interface is intimately related to the piezoelectric β-phase formation and depends on the ferrite type. The composite shows lower thermal stability due to the existence of mass loss processes at lower temperatures than the main degradation of the polymer induced by the presence of the ferrite fillers.

Acknowledgements We acknowledge the Foundation for Science and Technology (FCT) for financial support through PTDC/CTM/69316/2006 and NANO/NMed-SD/0156/2007 projects. P. M. and C. M. C thank the support of the FCT (grant SFRH/BD/45265/2008 and SFRH/BD/68499/2010). The authors also thank support from the COST Action MP1003, 2010 "European Scientific Network for Artificial Muscles."

References

1. Lovinger AJ (1982) In: Basset DC (ed) Developments in crystalline polymers. Elsevier, London
2. Lovinger AJ (1983) Science 220:1115
3. Martins P, Nunes JS, Hungerford G, Miranda D, Ferreira A, Sencadas V et al (2009) Phys Lett A 373:177
4. Martins P, Nunes JS, Hungerford G, Miranda D, Ferreira A, Sencadas V et al (2009) Phys Lett A 373:177

5. Ribeiro C, Sencadas V, Ribelles JLG, Lanceros-Mendez S (2010) Soft Mater 8:274
6. Gregorio JR, Cestari M (1994) J Polym Sci B: Polym Phys 32:859
7. Sencadas V, Gregorio R, Lanceros-Méndez S (2009) J Macromol Sci B 48:514
8. Yeow ML, Liu YT, Li K (2003) J Appl Polym Sci 90:2150
9. Lopes AC, Costa CM, Tavares CJ, Neves IC, Lanceros-Mendez S (2011) J Phys Chem C 115:18076
10. Pal K, Kang DJ, Zhang ZX, Kim JK (2009) Langmuir 26:3609
11. Yu S, Zheng W, Yu W, Zhang Y, Jiang Q, Zhao Z (2009) Macromolecules 42:8870
12. Martins P, Costa C, Lanceros-Mendez S (2011) Appl Phys A: Mater Sci Process 103:233
13. Greco T, Wang F, Wegener M (2010) Ferroelectrics 405:85
14. Sencadas V, Martins P, Pitaes A, Benelmekki M, Ribelles JLG, Lanceros-Mendez S (2011) Langmuir 27:7241
15. Martins P, Moya X, Phillips LC, Kar-Narayan S, Mathur ND, Lanceros-Mendez S (2011) J Phys D Appl Phys 44:1
16. Huang J-c, He C-b, Xiao Y, Mya KY, Dai J, Siow YP (2003) Polymer 44:4491
17. Wu B, Qi S, Wang X (2010) Polym Testing 29:717
18. He TS, Ma HH, Zhou ZF, Xu WB, Ren FM, Shi ZF et al (2009) Polym Degrad Stab 94:2251
19. Manna S, Batabyal SK, Nandi AK (2006) J Phys Chem B 110:12318
20. Peng Z, Kong LX (2007) Polym Degrad Stab 92:1061
21. Tang Y, Hu Y, Song L, Zong R, Gui Z, Chen Z et al (2003) Polym Degrad Stab 82:127
22. Schneider HA (1985) Thermochim Acta 83:59
23. Malik P, Castro M, Carrot C (2006) Polym Degrad Stab 91:634
24. Botelho G, Lanceros-Mendez S, Gonçalves AM, Sencadas V, Rocha JG (2008) J Non-Cryst Solids 354:72
25. Pramoda KP, Mohamed A, Phang IY, Liu TX (2005) Polym Int 54:226
26. Campos JSdC, Ribeiro AA, Cardoso CX (2007) Mater Sci Eng B: Solid State Mater Adv Technol 136:123
27. Zhong GJ, Zhang LF, Su R, Wang K, Fong H, Zhu L (2011) Polymer 52:2228
28. Chipara M, Lozano K, Hernandez A, Chipara M (2008) Polym Degrad Stab 93:871
29. Martins P, Costa CM, Benelmekki M, Botelho G, Lanceros-Mendez S (2012) CrystEngComm 14:2807
30. Kobayashi M, Tashiro K, Tadokoro H (1975) Macromolecules 8:158
31. Salimi A, Yousefi AA (2004) J Polym Sci B: Polym Phys 42:3487
32. Sencadas V, Gregorio R, Lanceros-Mendez S (2006) J Non-Cryst Solids 352:2226
33. Martins P, Costa CM, Lanceros-Mendez S (2011) Appl Phys A: Mater Sci Process 103:233
34. Badia JD, Moriana R, Santonja-Blasco L, Ribes-Greus A (2008) Macromol Symp 272:93
35. Chattopadhyay DK, Mishra AK, Sreedhar B, Raju K (2006) Polym Degrad Stab 91:1837
36. Broido A (1969) J Polym Sci A-2: Polym Phys 7:1761
37. Coats AW, Redfern JP (1964) Nature 201:68
38. Zulfiqar S, Rizvi M, Munir A (1994) Polym Degrad Stab 46:19
39. Silva MP, Sencadas V, Botelho G, Machado AV, Rolo AG, Rocha JG et al (2010) Mater Chem Phys 122:87
40. Oshea ML, Morterra C, Low MJD (1990) Mater Chem Phys 26:193
41. Chen D, Wang M, Zhang W-D, Liu T (2009) J Appl Polym Sci 113:644
42. Peeterbroeck S, Laoutid F, Taulemesse JM, Monteverde T, Lopez-Cuesta JM, Nagy JB et al (2007) Adv Funct Mater 17:2787
43. Yu LY, Shen HM, Xu ZL (2009) J Appl Polym Sci 113:1763
44. Jeon J-D, Kim M-J, Kwak S-Y (2006) J Power Sources 162:1304
45. Zheng MP, Gu MY, Jin YP, Jin GL (2000) Mater Sci Eng B: Solid State Mater Adv Technol 77:55
46. Li HF, Tan KY, Hao ZM, He GW (2011) J Therm Anal Calorim 105:357
47. Spencer TJ, Kohl PA (2011) Polym Degrad Stab 96:686
48. Min KD, Kim MY, Choi K-Y, Lee JH, Lee S-G (2006) Polym Bull 57:101
49. Chrissafis K, Bikiaris D (2011) Thermochim Acta 523:1
50. Jaleh B, Fakhri P, Noroozi M, Muensit N (2012) J Inorg Organomet Polym Mater 22:878
51. Kumar MNS, Yaakob Z (2009) J Appl Polym Sci 114:467
52. Lee JY, Liao YG, Nagahata R, Horiuchi S (2006) Polymer 47:7970
53. Yu JH, Huang XY, Wu C, Jiang PK (2011) IEEE Trans Dielectr Electr Insul 18:478